Cell Reports
Methods

Article

Long-term imaging of individual mRNA molecules in living cells

Graphical abstract

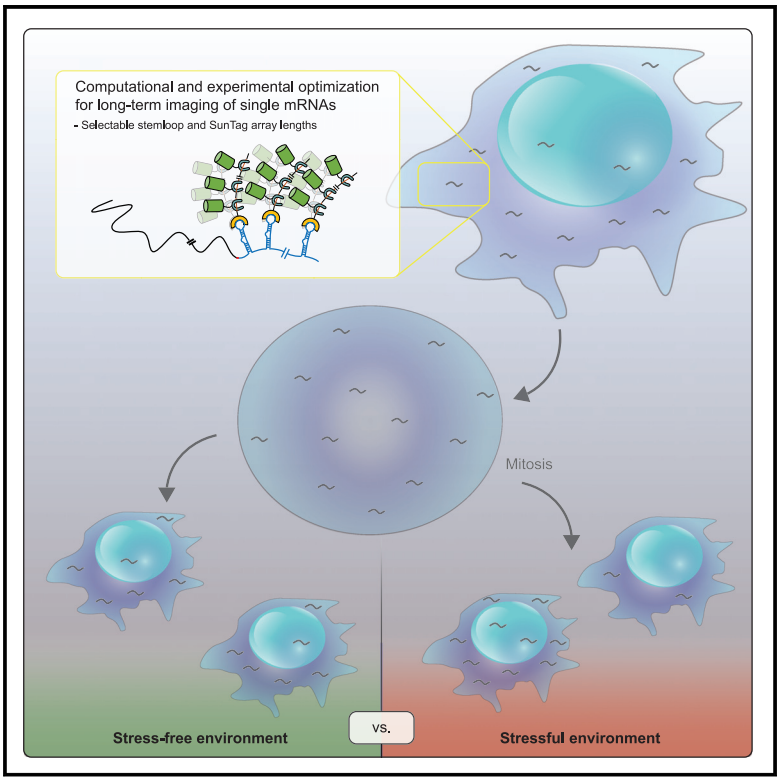

Authors

Yue Guo, Robin E.C. Lee

Correspondence

robinlee@pitt.edu

In brief

In this issue, Guo et al. use computational and experimental approaches to optimize an mRNA-labeling system that enables long-term imaging of single mRNA molecules in living cells. By tracking mRNA inheritance in cells undergoing mitosis, they show that environmental stresses promote diversity between mother-daughter and sister-cell pairs.

Highlights

- SunRISER is an approach for imaging single cytoplasmic mRNAs in living cells
- SunRISER-labeled mRNAs show high signal intensity and are resistant to photobleaching
- SunRISER is amenable to short stem-loop arrays without compromising mRNA detection
- Mitotic mRNA partitioning during stress increases diversity between sister cells

Guo & Lee, 2022, Cell Reports Methods 2, 100226
June 20, 2022 © 2022 The Author(s).
https://doi.org/10.1016/j.crmeth.2022.100226

CellPress

Cell Reports Methods

CellPress
OPEN ACCESS

Article

Long-term imaging of individual mRNA molecules in living cells

Yue Guo[1,2] and Robin E.C. Lee[1,3,4,*]
[1]Department of Computational and Systems Biology, School of Medicine, University of Pittsburgh, Pittsburgh, PA 15213, USA
[2]Department of Physics and Astronomy, University of Pittsburgh, Pittsburgh, PA 15260, USA
[3]Center for Systems Immunology, School of Medicine, University of Pittsburgh, Pittsburgh, PA 15213, USA
[4]Lead contact
*Correspondence: robinlee@pitt.edu
https://doi.org/10.1016/j.crmeth.2022.100226

MOTIVATION Determining the roles of mRNAs in rare events and dynamic spatiotemporal properties of mRNAs requires effective live-cell imaging techniques. Despite the emergence of many tools developed for enhancing signal intensity of labeling single mRNAs, there is still a lack of live-cell reporters to observe mRNAs by standard microscopy over long periods of time. We therefore developed a computationally and experimentally optimized method called SunRISER (SunTag-based reporter for imaging signal-enriched mRNA) that enables unambiguous live-cell detection of single mRNAs over timescales of hours to days.

SUMMARY

Single-cell imaging of individual mRNAs has revealed core mechanisms of the central dogma. However, most approaches require cell fixation or have limited sensitivity for live-cell applications. Here, we describe SunRISER (SunTag-based reporter for imaging signal-enriched mRNA), a computationally and experimentally optimized approach for unambiguous detection of single mRNA molecules in living cells. When viewed by epifluorescence microscopy, SunRISER-labeled mRNAs show strong signal to background and resistance to photobleaching, which together enable long-term mRNA imaging studies. SunRISER variants, using 8× and 10× stem-loop arrays, demonstrate effective mRNA detection while significantly reducing alterations to target mRNA sequences. We characterize SunRISER to observe mRNA inheritance during mitosis and find that stressors enhance diversity among post-mitotic sister cells. Taken together, SunRISER enables a glimpse into living cells to observe aspects of the central dogma and the role of mRNAs in rare and dynamical trafficking events.

INTRODUCTION

Messenger RNA (mRNA) molecules interact with RNA-binding proteins throughout their lifespan to carry genetic information and provide precise spatiotemporal regulation within cells. Live-cell single-molecule imaging techniques have enabled in-depth characterization of dynamics for mRNA-processing steps, including transcription, translation, splicing, export, degradation, and interactions with ribonucleoprotein (RNP) granules (Bertrand et al., 1998; Buxbaum et al., 2014; Czaplinski, 2017; Horvathova et al., 2017; Katz et al., 2016; Khuperkar et al., 2020; Larson et al., 2011; Mateju et al., 2020; Moon et al., 2019; Mor et al., 2010; Sato et al., 2020; Vargas et al., 2011; Vítor et al., 2019; Wan et al., 2021; Wang et al., 2016; Wilbertz et al., 2019; Wu et al., 2016; Yan et al., 2016). However, continuous imaging of single mRNAs has numerous challenges coupled to low imaging sensitivity that is exacerbated by rapid photobleaching (Pichon et al., 2018; Tutucci et al., 2018a). Typically, live-cell detection of single mRNAs requires sophisticated imaging approaches and trade-offs that restrict spatial and temporal aspects of imaging experiments.

Bacteriophage-derived MS2 and PP7 stem loops are extensively used for labeling mRNA molecules. In many applications, the reporter mRNA is tagged with 24× stem-loop copies in the 3′ UTR, and the corresponding coat protein (MCP or PCP) is fused with a fluorescent protein (FP). When co-expressed in the same cell, dimers of FP-fused coat proteins bind to each stem loop, enabling visualization of mRNAs and active transcription sites by fluorescence microscopy (Braselmann et al., 2020; Fusco et al., 2003; Rath and Rentmeister, 2015; Sato et al., 2020; Tutucci et al., 2018a; Vera et al., 2016). For most applications, coat proteins are also fused to a nuclear localization signal (NLS) to deplete unbound FP-MCP and -PCP from the cytoplasm, thereby increasing image contrast for mRNAs labeled in the cytoplasm (Ben-Ari et al., 2010; Ferguson and Larson, 2013; Lenstra and Larson, 2016; Spille and Kubitscheck, 2015;

This is an open access article under the CC BY-NC-ND license (http://creativecommons.org/licenses/by-nc-nd/4.0/).

Tutucci et al., 2018c; Wu et al., 2012). Since the NLS on unbound FP-M/PCP will favor a nuclear localization, the reduced availability of free coat proteins will limit cycling of FPs on cytoplasmic mRNAs. Consequently, depletion of fluorescence signals on cytoplasmic mRNA molecules resulting from dissociated and photobleached FP-M/PCP molecules is difficult to recover, which can constrain cytoplasmic mRNA detection over longer timescales. Although variants with increased stem-loop numbers enhance imaging sensitivity (up to 128 copies of extended MS2 repeats [Forero-Quintero et al., 2021; Golding and Cox, 2004; Tantale et al., 2016]), the bulky mRNA extension has the potential to perturb mRNA dynamics, and the reporter still suffers from photobleaching and limited resolution for single mRNAs.

Here, we develop and characterize SunRISER (SunTag-based reporter for imaging signal-enriched mRNA), an approach for long-term imaging of mRNA in living cells. SunRISER implements SunTag (Tanenbaum et al., 2014) as a scaffold to achieve fluorescence signal amplification of coat proteins and enhance contrast of mRNAs. Although the naive design is impractical, with inconsistent fluorescent properties that complicate mRNA detection, we optimize the approach using computational and synthetic biology to achieve robust and unambiguous detection of individual mRNAs. We show that SunRISER-labeled mRNAs are resistant to photobleaching over at least 7,000 exposures, and it is generalizable for robust whole-cell mRNA imaging experiments using PP7, MS2 (Chao et al., 2008), MS2V6, and MoonTag (Boersma et al., 2019; Tutucci et al., 2018b) as orthogonal components. We demonstrate that SunRISER variants using shorter 8× and 10× stem-loop arrays (SunRISER SRv.1.1 and SRv.1.2, respectively) result in consistent mRNA labeling and detection while reducing the size of alterations to target mRNA sequences. As an application of SunRISER, we characterize mitotic inheritance of mRNA molecules during a variety of stresses. When observed over the period of cell doubling time, we observe that mitotic mRNA inheritance is equally partitioned in standard growth conditions and that inflammatory stress or nutrient limitation can enhance diversity among post-mitotic sister cells. Our results demonstrate that SunRISER is an effective single-cell approach to investigate dynamics of mRNA molecules over long periods of time.

RESULTS

Design and model-based optimization of SunRISER

To facilitate long-term imaging of mRNAs in live cells, we set out to develop a signal-enrichment approach that circumvents several limitations associated with contemporary mRNA imaging techniques. To amplify fluorescence intensity of labeled coat proteins, our design employs SunTag, an array of GCN4 peptide epitopes that recruit multiple antibody molecules (Tanenbaum et al., 2014). The GCN4 antibody-peptide pair bind rapidly and serve as a robust scaffold for protein recruitment with a complex half-life in the order of minutes (Morfill et al., 2007; Weber-Bornhauser et al., 1998). Specifically, SunRISER comprises two stages of signal amplification: (1) 24× stem-loop copies are inserted in the 3′ UTR of mRNA and (2) the corresponding coat protein is fused with up to 24× SunTag peptides. With co-expression of an FP-fused single-chain antibody (scFv-GFP or codon-optimized scAB-GFP [Voigt et al., 2017]) that bind GCN4 epitopes, each SunTag coat protein can be labeled with up to 24 scFv-FPs, resulting in a theoretical upper bound of over 1,000 FP molecules per mRNA (24× stem loops, 2× coat proteins per stem loop, 24× SunTag arrays, 24 × 24 × 2 = 1,152 [Figure 1A]). In contrast with previous approaches, we reasoned that a two-stage approach where SunTag-fused coat proteins and scAB-GFP are both expressed throughout the cell would bolster active cycling of nascent coat proteins and antibody-FPs, providing resistance to photobleaching.

Our initial design for live-cell imaging of mRNAs was first aimed at circumventing problems associated with signal detection and cytoplasmic depletion of FP-fused coat proteins. We expressed components of the naive design in HeLa cells using 24 copies for both PP7 stem loops and SunTag arrays under control of the cytomegalovirus (cmv) promoter and imaged cells by 3D epifluorescence microscopy. As a generic transcript for mRNA detection, detection plasmids expressed a cyan FP (CFP) open reading frame, followed by 24×PP7 inserted after the stop codon in the 3′ UTR. Detection plasmids were transfected together with two additional plasmids expressing 24×SunTag-PCP and scFv-GFP.

Although diffraction-limited spots were visible, we observed spot-to-spot variability in size and intensity (Figures 1B and S1A). It was anticipated that two-stage signal amplification has non-linear systems properties, e.g., limiting scFv-GFP or excessive SunTag-PCP concentrations will both influence signal intensity dependent on mRNA concentration. We therefore developed a mathematical model (STAR Methods; Table S2) to estimate the number of FP molecules bound to mRNA for different expression levels of SunRISER components, scAB-GFP, SunTag-PCP, and PP7-tagged mRNA. Using protein-binding kinetics for SunRISER components and sampling across parameter combinations, we found broad variability in the expected intensity and signal to background (Figures 1C and S1), in some cases leading to a quantized distribution of single mRNA intensities (e.g., parameter combination 10). Variability between spots will complicate accurate identification and measurement of single mRNA molecules. By inspection, we found that a 5:1 ratio between scAB-GFP and SunTag-PCP with high-abundance expression yields uniform signal-intensity distributions in cells expressing up to 1,000s of mRNAs (Figure 1C). We also simulated 5×, 10×, and 24× SunTag-PCP variants. Although longer variants produce more intense signals, all had comparable signal-to-background ratios (Figure S1).

Refinement of SunRISER for whole-cell mRNA imaging

Guided by simulations, we designed SunRISER variants and assayed quantitative properties of mRNA spots. To establish an approximately 5:1 ratio of abundance for SunRISER protein components, we compared different constitutive promoters in HeLa cells (Figure S2A) predicted to have different strengths (Qin et al., 2010). Comparing cmv and ubc, promoters for strong and weak (respectively) mammalian gene expression, we found that the abundance of GFP expressed from the cmv promoter is approximately 5 times that of ubc (Figure S2A). To reduce the size of labeled mRNA complexes without significantly

CellPress
OPEN ACCESS

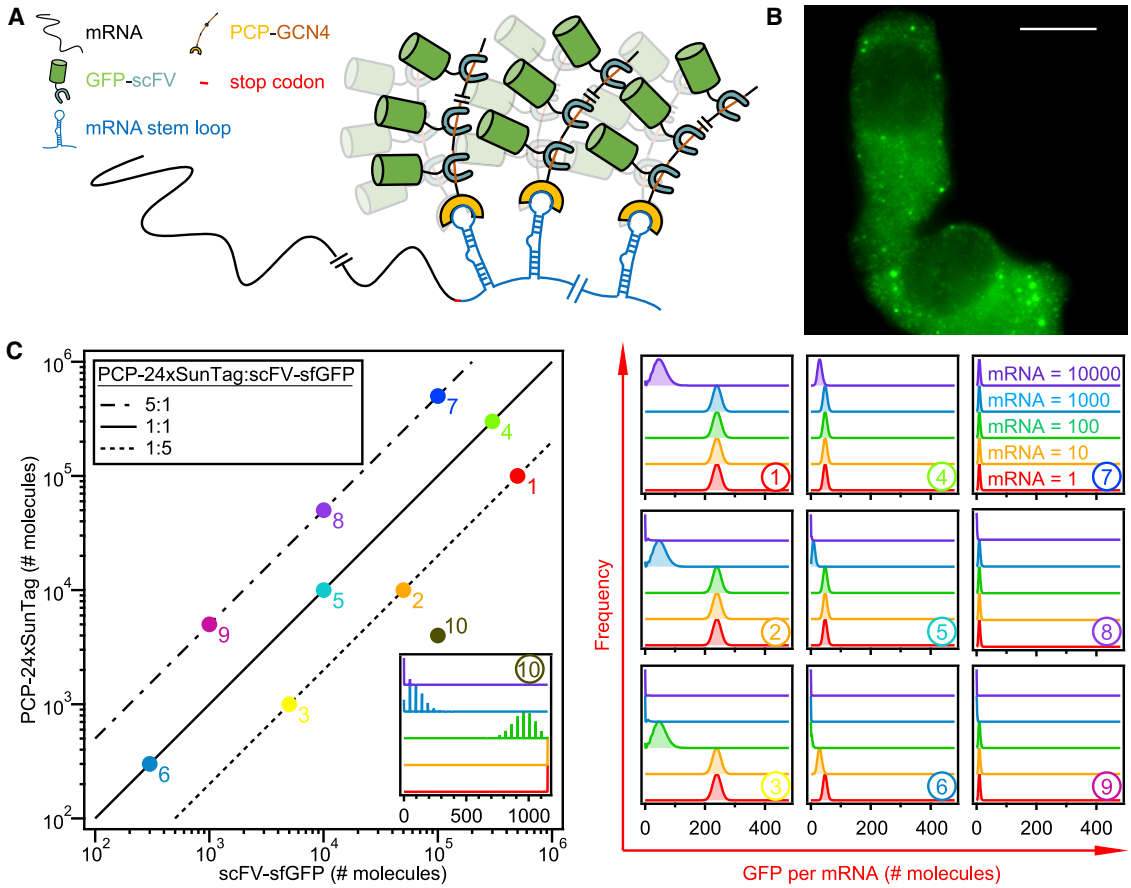

Figure 1. Design of SunRISER, a SunTag-based reporter for imaging signal-enriched mRNAs

(A) Design schematic of molecular components for the SunRISER strategy to image single mRNA molecules. An mRNA transcript (black) tagged at 3′ UTR with PP7 stem loops (blue) is bound by the PCP coat protein (yellow), which is fused to a SunTag GCN4 peptide array (orange). SunTag recruits GFP (green) through antibody-peptide-specific binding between scFv (gray) and GCN4 epitopes.

(B) Maximum intensity projection of z stacks for representative HeLa cells 24 h after transfection with three plasmids: phage-cmv-cfp-24×pp7, cmv-24×SunTag-PCP, and cmv-sfGFP-GB1-scAB. Scale bar: 10 μm.

(C) Parameter sweeps in the space spanned by number of molecules for scFv-GFP and 24×SunTag-PCP (left) using a computational model to calculate number of GFP molecules per mRNA. Parameter combinations 1–10 were selected to represent different ratios between scFv-GFP and 24×SunTag-PCP (solid line 1:1, dotted line 5:1, and dash-dotted line 1:5), and different expression levels and frequency plots are shown (right). Different concentrations of mRNAs per cell are distinguished by different colors.

See also Figures S1 and S2 and Table S2 for binding constants.

compromising signal to background (Figure S1D), we validated model predictions using 10xSunTag-PCP. HeLa cells were co-transfected with SunRISER components, approximating parameter combinations 1, 4, 6, and 9 (Figures 1 and S1). Consistent with simulations, an approximately 5:1 ratio achieved by cmv-scAB-GFP and ubc-SunTag-PCP (Figure S2C) enhanced signal intensity and signal-to-background values compared to sub-optimal ratios (Figures S2B, S2D, and S2E) that fail to reliably and unambiguously label single transcripts driven by the same cmv promoter. Using single-molecule fluorescence *in situ* hybridization (smFISH) against PP7 stem-loop sequences (Heinrich et al., 2017) in SunRISER-expressing cells, we confirmed co-localization of cytoplasmic mRNAs between SunRISER and smFISH. However, smFISH revealed nuclear mRNAs that were not detected by SunRISER (Figure S3A). Further live-cell and fixed-cell assays demonstrated that GFP-SunTag-PCP is excluded from the nuclear compartment (Figures S3B and S3C), suggesting that SunTag-PCP required further optimization for whole-cell mRNA detection.

To alleviate nuclear-export effects from repeats of the GCN4 epitope and cytoplasmic sequestration of anti-GCN4 (Wörn et al., 2000), we continued with the smaller 5xSunTag variant. Next, we focused on modifications to 5×SunTag-PCP for homogeneous expression throughout the cell and for detection of nuclear and cytoplasmic mRNAs. We also considered that the ornithine decarboxylase (ODC) tag (Kahana et al., 2005) fused to SunTag-PCP while under the control of the cmv promoter as an alternative approach to establish a 5:1 deficit of SunTag-PCP that may also alter its subcellular distribution. ODC is one of the most short-lived proteins, which can facilitate fast degradation of tagged proteins. Although ODC tagging is not as precise as controlling transcript abundance using promoters, ODC

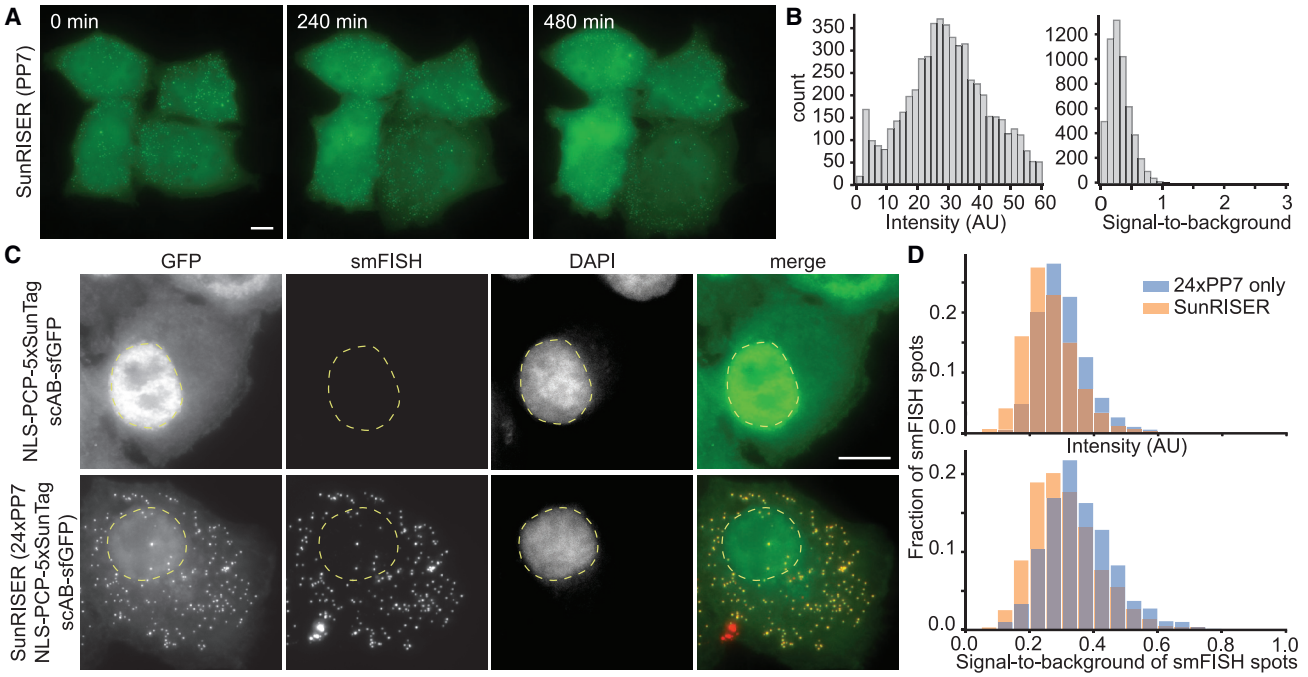

Figure 2. The optimal SunRISER design allows long-term imaging of single mRNA molecules throughout the cell

(A) Maximum intensity projections of HeLa cells transfected with SunRISER, consisting of the detection plasmid phage-cmv-cfp-24×pp7, as well as ubc-nls-PCP-5×SunTag and cmv-sfGFP-GB1-scAB. Cells were imaged by 60× widefield fluorescence microscopy for 8 h with a 10 min framerate. Scale bar: 10 μm. See also Video S1.

(B) Histograms of signal intensity and signal-to-background ratio of SunRISER-labeled single mRNAs quantified with dNEMO (Kowalczyk et al., 2021). Signal intensity is defined as the average of background-corrected pixel values within the area of each detected spot. Signal-to-background ratio is calculated as the ratio of average pixel intensity within an mRNA spot divided by the average intensity of background pixels in an annular ring surrounding the spot (n = 23 for cell numbers and n = 5,611 for spots numbers).

(C) Maximum intensity projection images of smFISH performed with probes against the PP7 stem loops in HeLa cells transfected with SunRISER protein components (ubc-nls-PCP-5×SunTag and cmv-sfGFP-GB1-scAB) only (top) or complete SunRISER with detection plasmid (bottom). Scale bar: 10 μm. See also Figures S2–S4.

(D) Histograms of signal intensity and signal-to-background ratio for single mRNAs labeled with smFISH Q670 probes against the mCherry coding sequence in cells expressing phage-cmv-mCherry-24×pp7 detection plasmid without (blue, n = 10 for cell numbers and n = 2,156 for spots numbers) and with (orange, n = 11 for cell numbers and n = 2,842 for spots numbers) remaining SunRISER components.

fusion of SunTag-PCP is a viable approach to limit its expression relative to scAB-GFP. Although several variants enable whole-cell mRNA detection, an optimized design was eventually achieved by switching the fusion order of PCP and 5×SunTag, in addition to inserting a 5′ NLS (Figures S3D and S3E; Table S1). We note that the addition of a 5′ NLS without switching the fusion order to PCP-SunTag still fails to detect nuclear mRNAs when expressed with other SunRISER components.

The optimized SunRISER version 1 (SRv.1) design consists of three plasmids (cmv-GFP-GB1-scAB, phage-nls-PCP-5×SunTag, and a detection plasmid expressing mRNA tagged with 24XPP7) and has an overall molecular weight comparable with MS2x128 (Table S3). SunRISER faithfully labels single mRNAs in the nucleus and cytoplasm with uniform fluorescence intensity and high signal to background, allowing for long-term imaging (Figure 2; Video S1). We also compared fluorescence distributions of single cytoplasmic mRNAs detected by smFISH in cells expressing either the detection plasmid only or the complete SunRISER system. We found that expression of SunRISER components does not significantly alter the fluorescence intensity and signal to background of mRNA spots (Figure 2D), suggesting that each SunRISER spot represents a single mRNA molecule. Similarly, detection plasmids using weak and strong promoters to express low and high mRNA numbers result in expected mRNA abundances, consistent fluorescence intensity, and signal to background, in line with expectations from the model (Figures S4A–S4C). For some cell lines, calibration of promoters for protein components may be necessary to ensure optimal SunRISER labeling. Nevertheless, even though promoter activity will vary by cell type, expression of SRv.1 components in A549 cells produced qualitatively similar results even though A549 cells are phenotypically distinct from HeLa by many criteria (Figure S4D). Furthermore, the same optimization can be applied to orthogonal stem loops and antibody-epitope pairs, such as MS2, MS2V6 (Tutucci et al., 2018b), and MoonTag (Boersma et al., 2019) (Figures 3 and S5).

Characterization of optimal SunRISER system

To compare SunRISER directly with widely used approaches, we imaged cells expressing the 24xpp7 detection plasmid with

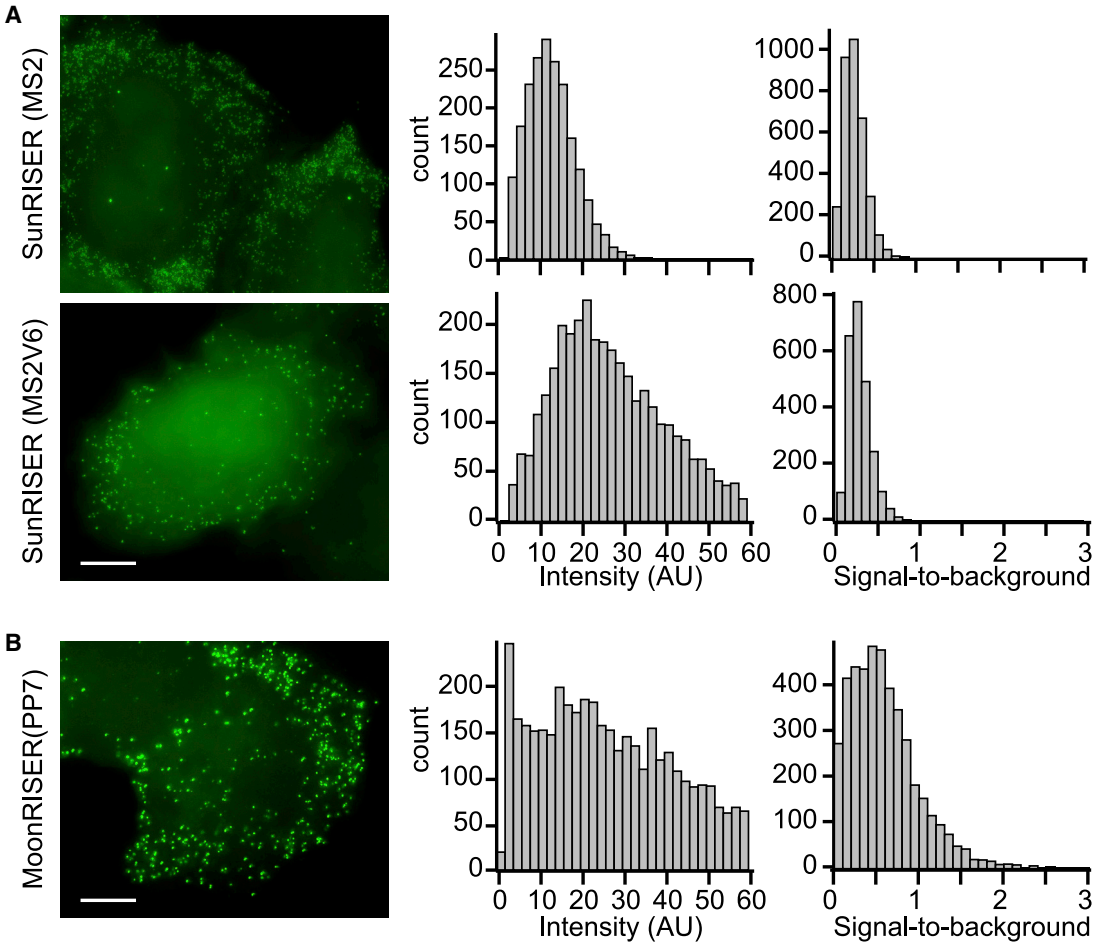

Figure 3. Design principles of SunRISER are generalizable to orthogonal stem loops and protein-tagging systems

(A) HeLa cells transfected with detection plasmids phage-cmv-CFP-24×MS2 (top) and phage-cmv-CFP-24×MS2V6 (bottom) stem-loop variants of SunRISER with ubc-nls-MCP-5×SunTag show similar characteristics and intensity distributions, quantified in histograms (right, top: n = 30 for cell numbers and n = 8,227 for spots numbers; bottom: n = 21 for cell numbers and n = 4,627 for spots numbers).

(B) HeLa cells transfected with detection plasmid phage-cmv-cfp-24×pp7 with cmv-sfGFP-GB1-Nb-gp41 and ubc-nls-PCP-12×MoonTag, quantified in histograms (right, n = 19 for cell numbers and n = 4,534 for spots numbers). We note that the MoonRISER example can be further optimized as it uses a longer 12× MoonTag and a nanobody that has different binding properties. Cells were imaged with 60× wide-field microscope 24 h after transfection and quantified with dNEMO (Kowalczyk et al., 2021) Scale bar: 10 μm.

See also Figure S5.

PCP-GFP. Signal-to-background for standard PP7-labeling was near the detection limit throughout, and most cytoplasmic mRNAs fell below detectable signal levels within 10 min of imaging (Figure S6). By contrast, signal intensity and signal-to-background for SunRISER remained strong and consistent between single cells throughout the 10-min experiments (Figures S6C and S6D). To characterize photobleaching properties of SunRISER in more challenging imaging conditions, cells were exposed to a rapid time-lapse experiment where 7200 consecutive epifluorescence images were collected within 1 h (Figure 4). Although signal intensity values decreased to approximately 40% by the end of the experiment, the signal-to-background was reduced only modestly, and mRNAs were robustly detected in single cells throughout (Figures 4B and 4C). Taken together, we conclude that SunRISER is resistant to photobleaching and provides greater robustness for detection of mRNAs when compared with the well-established PP7-PCP systems.

Next, we compared functional properties of SunRISER-labeled mRNA with expectations from unlabeled mRNA, as well as previous reports from the literature. Comparing mCherry fluorescence expressed from a detection plasmid in single cells from a transcript with 24×PP7 stem loops, SunRISER labeling did not have significant effects on protein production (Figure S7A). SunRISER-labeled mRNA maintained a mean ratio of 5 between nuclear and cytoplasmic compartments (Figure S7B), which is consistent with mean value expectations of 3.8–6.5 based on RNAseq of subcellular fractions (Bahar Halpern et al., 2015), suggesting the subcellular distribution of SunRISER-labeled mRNA is unaltered. Remarkably, SunRISER-labeled mRNA numbers in response to transcription

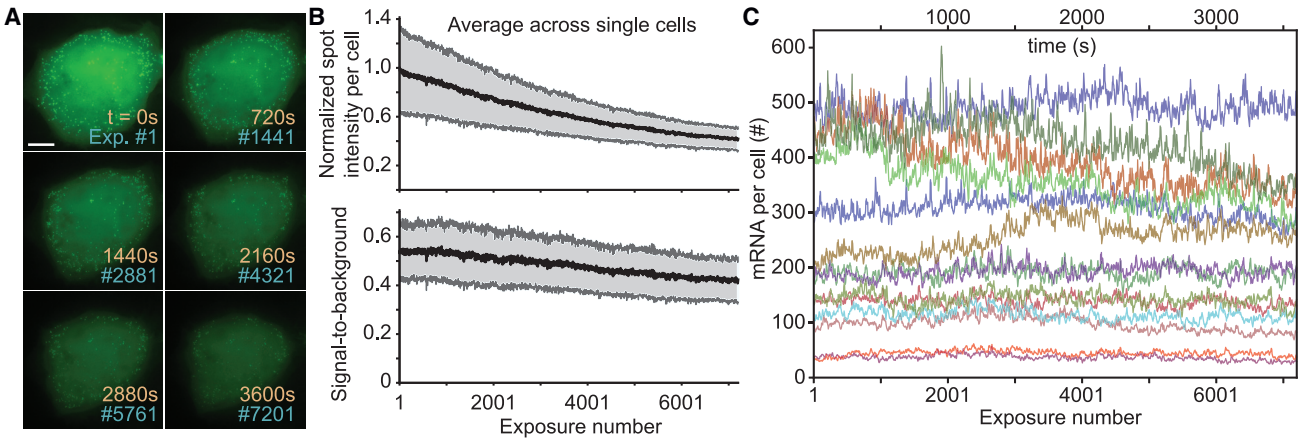

Figure 4. SunRISER is resistant to photobleaching and robustly labels mRNA molecules during prolonged imaging conditions

(A) Maximum intensity projections of SunRISER SRv.1-labeled mRNAs at different time points. Twenty-four h after transfection of HeLa cells with detection plasmid phage-cmv-cfp-24×pp7 with ubc-nls-PCP-5×SunTag and cmv-sfGFP-GB1-scAB (SunRISER), cells were imaged by 60× wide-field fluorescence microscopy as 4× frame z stacks at 2 s intervals over a 1 h duration. Scale bar: 10 μm.

(B) Time course of normalized signal intensity (top) and signal-to-background values (bottom) for spots labeled with SunRISER across different single cells (n = 14). Solid line marks the mean signal intensity and mean signal-to-background values averaged among single cells (signal intensity was normalized by the average spot intensity across cells at the first frame of imaging), and shaded area indicates the standard deviation between single cells.

(C) Time course of mRNA counts for 1 h fast movies across different cells. The counts were smoothed by a sliding window of 5 frames.

See also Figures S6 and S7.

inhibition revealed mRNA half-lives with significant cell-to-cell variability (Figure S7C). Single cell mRNA half-lives were consistent with previous results, spanning the divide that separates median mRNA half-lives expected of stable and unstable mRNA molecules (Schwanhäusser et al., 2011; Tani et al., 2012). Although this may represent a source of cellular heterogeneity, cells with particularly long mRNA half-lives can also indicate partial escape from transcriptional inhibition through enhanced chemical efflux or other mechanisms that also vary between cells. Finally, extended extensions of widely used RNA tags have the potential to alter diffusion rates, so we also measured diffusive properties of SunTag-labeled mRNA. Since the SunRISER-labeled mRNA complex is larger than 24×PP7-PCP (Table S3), it is expected to result in lower single-mRNA diffusion rates within the cell. When measured from high-frequency time-lapse images, diffusive motion of SunRISER-labeled mRNA molecules was 0.19 $\mu m^2/s$ (Figures S7D–S7F), which is lower yet within the expected range of values (0.15–0.72 $\mu m^2/s$) measured from 24×PP7-PCP-labeled endogenous mRNAs (Wu et al., 2012). Taken together, although the SunRISER mRNA-protein complex is bulkier, it does not significantly alter mRNA function beyond expectations from previous analysis of conventional fluorescent mRNA reporters (Braselmann et al., 2020).

SunRISER variants with small stem-loop arrays and reduced plasmid requirements

Most mRNA-tagging applications using bacteriophage-derived stem loops use a 24× copy array or larger for signal amplification. Shorter stem-loop arrays exist but are often used in CRISPR-based genome imaging, where multiple copies of target sites are present to detect bright foci, or are engineered to reduce impact on general mRNA metabolism (Katz et al., 2021; Ma et al., 2018; Saroufim et al., 2015). We therefore asked whether SunRISER can be used to label single mRNAs using shorter stem-loop arrays.

To establish versatility of our approach, we developed SunRISER configurations using shorter PP7 stem-loop arrays (8×, 10×, 12×) and varying lengths of PCP-SunTag arrays (5×, 10×, 12×, and 24×). For each array combination, we measured median and variance of signal to background for distributions of single mRNA molecules (Figure 5 and S8A). We found that although longer SunTag arrays tend to correspond with greater signal to background, they also result in greater inter-spot variance, which reduces mRNA-detection efficiency (Figures 5A and 5B). Of all combinations tested, we found two SunRISER variants capable of labeling mRNAs with low variance, comparable signal to background, and comparable mRNA detection numbers to SunRISER (Figures 5A, 5B, S8B, and S8C). We refer to these as SRv.1.1 and SRv.1.2 respectively for 8×PP7 with 10×SunTag and 10×PP7 with 12×SunTag. Although mRNA labeled with SRv.1, SRv.1.1, and SRv.1.2 have comparable molecular weights to MS2x128 (Table S3), these alternative designs provide flexibility in SunRISER applications to label shorter mRNAs without compromises to mRNA detection.

Finally, to further enhance versatility of the SunRISER approach, we considered whether the protein components of SunRISER can be expressed from a single plasmid with multiple promoters. We generated a plasmid with two components to independently regulate expression of GFP-scAB and PCP-5×ST, thereby in combination with the detection plasmid reducing the system to two plasmids (referred to as SRv.1-2P; Figure 5C). Single mRNAs detected using the SunRISER variant

CellPress
OPEN ACCESS

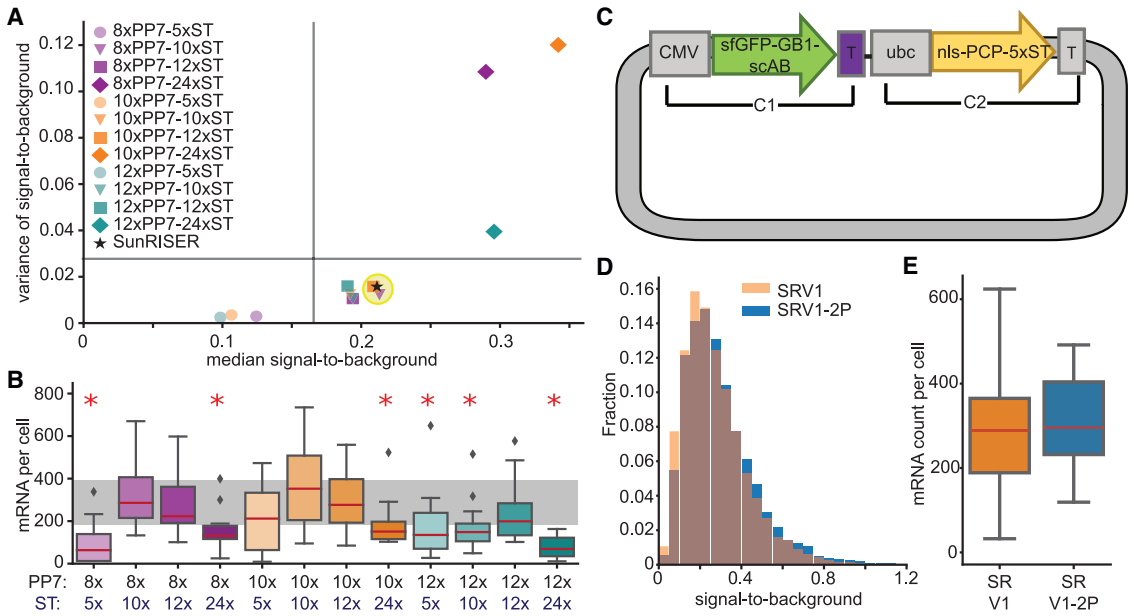

Figure 5. Design of SunRISER variants

(A) Scatterplot of variance and median for signal-to-background ratio of single mRNAs labeled with different combinations of PP7 stem-loop and SunTag arrays. Vertical and horizontal lines mark the preferred region in the bottom-right quadrant with small inter-spot variance and strong signal. Optimized SunRISER SRv.1 is indicated with a star.

(B) Boxplots for mRNA numbers detected by different combinations of PP7 stem-loop and SunTag arrays. Gray region marks the first and third quantiles for mRNA numbers detected by optimal SunRISER SRv.1. Configuration with significantly different mRNA numbers from SRv.1 are indicated with red stars ($p < 0.05$, two-tailed t test).

(C) Diagram of single plasmid encoding 2 protein components (C1) cmv-sfGFP-GB1-scAB and (C2) ubc-nls-PCP-5×SunTag for the SunRISER SRv.1-2P variant.

(D and E) Histograms of signal-to-background ratio (D) and boxplots of mRNA numbers (E) in cells labeled with SunRISER variants SRv.1 (n = 26 for cell numbers and n = 8,713 for spots numbers) and SRv.1-2P (n = 23 for cell numbers and n = 8,875 for spots numbers).

See also Figure S8.

SRv.1-2P again showed comparable imaging and detection properties to SRv.1 (Figures 5D, 5E, and S8D). As expected, SRv.1.1-2P and SRv.1.2-2P also produce results that are indistinguishable from their 3-plasmid counterparts.

Variability of mitotic mRNA inheritance between sister cells

Random partitioning of biomolecules between daughter cells during cell division is a contributing source to non-genetic heterogeneity (Huh and Paulsson, 2011a, 2011b). The symmetry of mRNA inheritance during mitosis is tightly regulated during embryonic development and tissue homeostasis as the distribution of specific mRNAs controls cell-signaling pathways and subsequent cell-fate decisions (Shlyakhtina et al., 2019; Skamagki et al., 2013; Stahl et al., 2019; Sunchu and Cabernard, 2020; Varela et al., 2016). However previous studies on mRNA division have been performed mostly across populations and in fixed samples, therefore lacking the resolution to examine mRNA partitioning in single mother and daughter cells in real time. Since SunRISER is theoretically capable of imaging mRNAs over timescales of cell division, we set out to quantify mRNA partitioning between single mother-daughter- and sister-cell pairs in various growth conditions.

Enabled by the long-term mRNA imaging capability of SunRISER, we imaged HeLa cells transfected with cmv-promoter-driven mRNAs labeled with SunRISER for 24 h and quantified mRNA abundance during cell division with and without cellular stress (Figures 6A and 6B; Video S2). SRv.1-labeled mRNAs that encode CFP were used to examine the mitotic partitioning mechanisms for a generic mRNA species that is not subject to particular mitotic regulation mechanisms. The relative difference in mRNA levels between sister cells was used as a metric for symmetry of mRNA partitioning. We observed significant variability between pairs of sister cells in the same culture condition (Figures 6 and S9). To classify differences between sister-cell pairs, we used information criteria and k-means clustering (Figures S9A and S9B) and found 4 clusters that we refer to as "symmetric," "weak asymmetry," "asymmetric," and "strong asymmetry." Cells cultured in the presence of tumor necrosis factor (TNF; 15 ng/mL) or low-serum conditions (5% FBS) showed a significant shifts favoring asymmetric with the emergence of rare sister-cell pairs with strong asymmetry (Figures 6C and S9B). We further compared mRNA ratios between the sum of daughter cells and their corresponding mother (Figure 6D) and observed evidence of significant mitotic transcription (defined as mRNA ratio significantly greater than 1 for the sum of daughter cells divided by the mother cell) induced by cells exposed to lithium chloride (LiCl) as well as low-serum conditions (Figures 6D, S9C, and S9D). Notably, although LiCl promoted escape from silencing of mitotic transcription, it only had modest effects on

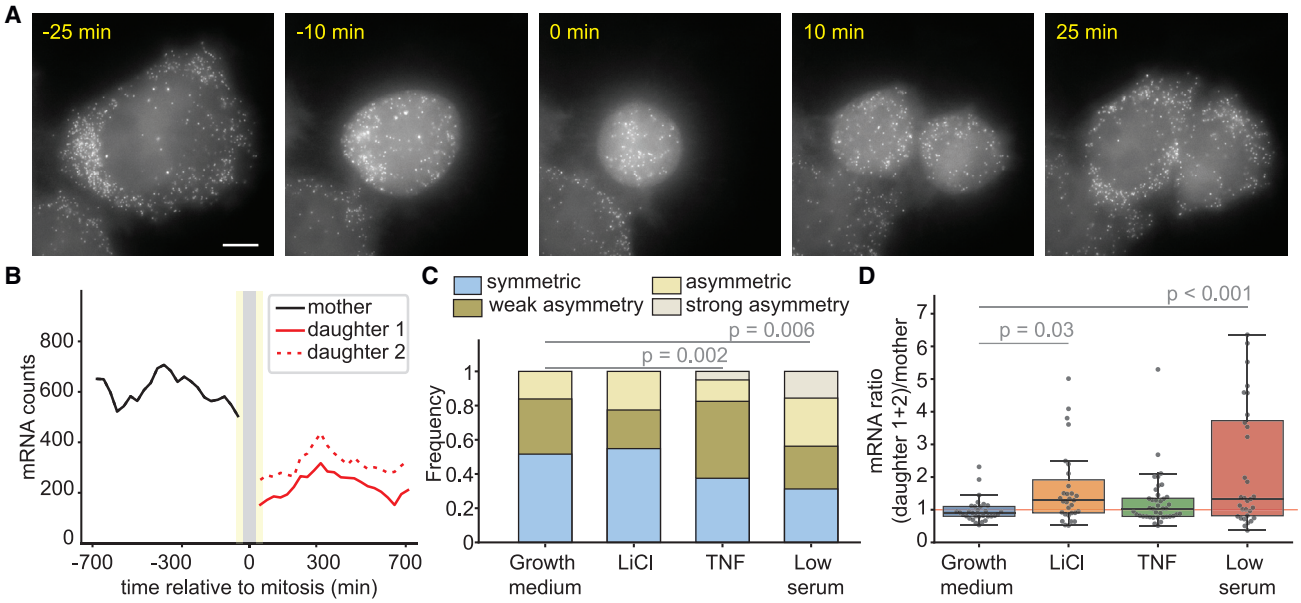

Figure 6. Long-term imaging to monitor mRNA partitioning during cell division

(A) Time course for maximum intensity projection images of HeLa cells expressing SunRISER SRv.1 in standard growth medium undergoing mitosis. Frame 0 is the last frame where mother cell remains as a single cell with a semi-detached circular appearance. Cells were imaged for 24 h with a 10 min frame rate. See also Video S2.

(B) Representative trajectories of mRNA counts during mitosis for the cell depicted in panel (A). Solid black line marks mRNA numbers for the mother cell, and red lines indicate mRNA numbers for each daughter cell. Gray bar marks the window around frame 0 during which time mRNA counts are not accurate due to morphological changes and temporary detachment of the dividing cell (see also STAR Methods). Yellow bars mark the 3 frame window used for extraction of mRNA counts for mother and daughter cells in subsequent analysis.

(C) Bar graphs for relative difference of mRNA between sister cells during mitosis when cells are cultured in media without or with indicated stress. Classifications are based on information criteria and k-means clustering (see also Figure S9). Yellow-colored bars indicate the fraction of cells identified as undergoing asymmetric division with different shades representing the indicated subcategories. Blue-colored bars indicate the symmetric division category. p value was calculated using the Levene test.

(D) Boxplots of ratios for the sum of post-mitotic daughter mRNAs divided by the mRNA number for the pre-mitotic mother cell. Media composition without or with stress is as indicated. Black dots represent individual sister pairs. Red line marks ratio value equal to 1. p value was calculated using 2-tailed t tests. Outliers with more than 8-fold increase in transcript numbers are not plotted.

See also Figure S10.

asymmetric mRNA inheritance between post-mitotic sister cells (Figures 6 and S9D). For all environmental stresses, distributions of mRNAs allocated to daughter cells shifted significantly away from the binomial distribution observed for cells dividing in the growth medium condition (Figure S10A). Although R^2 values suggest that partitioning of mRNA between daughter cells is partly explained by distribution of total cellular mass (Figure S10B), our data suggest that other factors also contribute to the observed diversification between sister cells.

DISCUSSION

The lifespan of mRNA molecules in mammalian cells occurs over timescales of hours to days, during which mRNAs participate in highly dynamic processes that are tightly regulated in time and space. Bacteriophage-derived stem loops and FP-tagged coat proteins are current state-of-the-art approaches to detect single mRNA molecules in live cells; however, there are still significant limitations of these seminal reporter systems. Furthermore, to take full advantage of typical stem-loop- and coat-protein-labeling systems requires highly customized microscopy equipment. For example, two-photon fluorescence fluctuation spectroscopy can provide accurate measurement of single mRNAs up to several minutes, but these measurements cannot be sustained over longer durations (Tutucci et al., 2018a). By contrast, SunRISER enables long-term investigation of dynamical mechanisms of mRNAs over timescales of at least 24 h using standard epifluorescence microscopy.

To optimize SunRISER, simulations were used to explore nonlinear interrelations between the components of the two-stage reporter system. As a static model, we assume that all binding events in the system have reached equilibrium. The steady-state assumption allows conversion of binding affinity to binding probabilities, which reduces the computational load while preserving key features of the system. Selected binding constants for our simulations were chosen specific to stem-loop, coat-protein, and antibody-epitope pairs used in this study (summarized in Table S2). With appropriate modifications to the kinetic parameters, the mathematical model (https://github.com/recleelab/SunRISER_SupplementalModel) is generalizable to any two-stage molecular amplification reporter and is extensible to higher-order systems.

Direct comparison between SunRISER and PP7-PCP systems showed significant improvements to signal intensity, stability, and signal-to-background ratios. Furthermore, SunRISER minimally perturbs normal mRNA function and is highly resistant to photobleaching. Although our stress-test and long-term experiments concluded after 7,200 consecutive images and 24 h, respectively, we expect that these represent lower limits and that mRNA signals will remain detectable over longer repeat-exposure conditions. We also note that several "sub-optimal variants" of the PCP-SunTag component of SunRISER that were tested in our synthetic biology approach showed an exclusively cytoplasmic localization (Table S1). Although these sub-optimal variants of the reporter do not identify nuclear mRNAs, they may still have value in certain experimental settings where selective labeling of only cytoplasmic mRNAs is preferred. Finally, SunRISER variants SRv.1, SRv.1.1, and SRv.1.2 offer flexibility to label shorter mRNAs by balancing the reporter's mRNA:protein composition, reducing sequence perturbations on mRNAs without compromising signal to background and detection.

Asymmetric mitotic mRNA inheritance is an essential mechanism to control the maintenance and emergence of specialized cellular phenotypes during development (Skamagki et al., 2013; Varela et al., 2016). Previous studies on mRNA partitioning during mitosis typically required cell fixation and chemical synchronization, with mRNA levels assessed via bulk cell measurements that are incapable of providing dynamical single-cell information. Here, we used SunRISER to visualize the mRNA partitioning during mitosis in single cells without chemical perturbations associated with synchronization. We observed significant heterogeneity between sister cells in terms of mRNA partitioning during both TNF stimulation and in low-serum conditions. Remarkably, upon serum starvation, a distinct population of cells that exhibit very strong asymmetry in mRNA partitioning arises concomitant with evidence for active mitotic transcription. We surmise that asymmetric segregation of mRNA and rapid divergence via mitotic transcription is a strategy to increase molecular diversity in the cell population. Similar bet-hedging strategies have been observed in yeast and attributed to asymmetric mitotic inheritance of proteins (Levy et al., 2012), imparting increased fitness to more diverse populations growing in harsh environments. During stress, such as nutrient limitation, asymmetric partitioning of mRNA in mammalian cells may similarly enhance population-level fitness via diversification of cellular states.

In summary, SunRISER enables unambiguous detection of mRNA molecules in living cells. By using an optimized two-phase design, our reporter system is robust to photobleaching over long-term experiments, and the approach is generalizable to other stem-loop and peptide arrays using the accompanying computational tool. We anticipate that this approach will facilitate studies of dynamical properties for single mRNAs and biological variability between single cells, cell types, and eventually in tissues, with applications across biological disciplines.

LIMITATIONS OF THE STUDY

While SunRISER presents a solution for robust labeling of single mRNAs in mammalian cells, there are limitations to be considered. Optimal mRNA labeling with SunRISER requires an expression ratio of protein components using promoters that may be diversely regulated in different cell types and may also vary in different environmental conditions. When applying SunRISER to a new cell line, a stable cell line, or to certain environmental conditions that impact mRNA detection, it may be necessary to test different promoters to ensure the optimal expression ratio is achieved. In our application of SunRISER to study mRNA partitioning during mitosis, a generic transcript was used to examine passive mechanisms of mitotic inheritance of mRNAs. Expectations for mRNA distributions between daughter cells may change significantly for mRNAs associated with specific functions such as mitosis, development, and cell-fate specification. Furthermore, SunRISER-labeled transcripts comprise a large complex that does not significantly alter normal function of mRNAs assessed here but may still affect other dynamical properties of mRNAs, for example, structural complexes or particular biological processes. When mRNA translation and stability are important aspects of a study, careful controls should be performed to verify there are no specific effects from SunRISER labeling on the particular mRNA species. Therefore, other mRNA-labeling methods such as 24×PP7/PCP-GFP may be more appropriate for applications that do not require imaging of cytoplasmic mRNAs, long-term processes, or rapid assemblies such as transcriptional start sites. When SunRISER is used to study mRNA-mRNA interaction or stoichiometry relations, verification via orthogonal approaches will be necessary. Finally, we note that simulations predict SunRISER will perform poorly at extremely high mRNA-expression levels (Figure 1C). Caution on interpretation should be taken when mRNA numbers exceed 1,000s per cell or for applications where large numbers of mRNAs are bundled in close proximity.

STAR★METHODS

Detailed methods are provided in the online version of this paper and include the following:

- KEY RESOURCES TABLE
- RESOURCE AVAILABILITY
  - Lead contact
  - Materials availability
  - Data and code availability
- EXPERIMENTAL MODEL AND SUBJECT DETAILS
- METHOD DETAILS
  - Plasmid construction
  - Live cell imaging and quantification of single mRNA spots with dNEMO
  - Stress treatments
  - smFISH probes and image acquisition
  - Fixed-cell immunofluorescence
- QUANTIFICATION AND STATISTICAL ANALYSIS
  - Statistical analysis
  - Half-life and diffusion constant measurement
  - mRNA inheritance during mitosis analysis
  - Model-based calculation of signal intensity and signal-to-background values

SUPPLEMENTAL INFORMATION

Supplemental information can be found online at https://doi.org/10.1016/j.crmeth.2022.100226.

ACKNOWLEDGMENTS

We thank Gabriel Kowalczyk and other members of the Lee lab, in addition to Drs. Yi-Jiun Chen, Xiao-lun Wu, and Qiuhong Zhang, for many helpful discussions. This work was supported by generous funding to R.E.C.L. from NIH grant R35-GM119462 and the Alfred P. Sloan Foundation.

AUTHOR CONTRIBUTIONS

Conceptualization, Y.G. and R.E.C.L.; methodology, Y.G. and R.E.C.L.; investigation, Y.G.; software, Y.G.; formal analysis, Y.G.; writing – original Draft, Y.G. and R.E.C.L.; writing – review & editing, Y.G. and R.E.C.L.; visualization, Y.G. and R.E.C.L.; funding acquisition, R.E.C.L.; supervision, R.E.C.L.

DECLARATION OF INTERESTS

The authors declare no competing interests.

Received: October 14, 2021
Revised: March 10, 2022
Accepted: May 4, 2022
Published: May 25, 2022

REFERENCES

AAT Bioquest Inc (2022). Quest CalculateTM RNA Molecular Weight Calculator. AAT Bioquest. https://www.aatbio.com/tools/calculate-RNA-molecular-weight-mw.

Bahar Halpern, K., Caspi, I., Lemze, D., Levy, M., Landen, S., Elinav, E., Ulitsky, I., and Itzkovitz, S. (2015). Nuclear retention of mRNA in mammalian tissues. Cell Rep. *13*, 2653–2662. https://doi.org/10.1016/j.celrep.2015.11.036.

Ben-Ari, Y., Brody, Y., Kinor, N., Mor, A., Tsukamoto, T., Spector, D.L., Singer, R.H., and Shav-Tal, Y. (2010). The life of an mRNA in space and time. J. Cell Sci. *123*, 1761–1774. https://doi.org/10.1242/jcs.062638.

Bertrand, E., Chartrand, P., Schaefer, M., Shenoy, S.M., Singer, R.H., and Long, R.M. (1998). Localization of ASH1 mRNA particles in living yeast. Mol. Cell *2*, 437–445. https://doi.org/10.1016/S1097-2765(00)80143-4.

Boersma, S., Khuperkar, D., Verhagen, B.M.P., Sonneveld, S., Grimm, J.B., Lavis, L.D., and Tanenbaum, M.E. (2019). Multi-color single-molecule imaging uncovers extensive heterogeneity in mRNA decoding. Cell *178*, 458–472.e19. https://doi.org/10.1016/j.cell.2019.05.001.

Braselmann, E., Rathbun, C., Richards, E.M., and Palmer, A.E. (2020). Illuminating RNA biology: tools for imaging RNA in live mammalian cells. Cell Chem. Biol. *27*, 891–903. https://doi.org/10.1016/j.chembiol.2020.06.010.

Buxbaum, A.R., Wu, B., and Singer, R.H. (2014). Single β-actin mRNA detection in neurons reveals a mechanism for regulating its translatability. Science *343*, 419–422. https://doi.org/10.1126/science.1242939.

Chao, J.A., Patskovsky, Y., Almo, S.C., and Singer, R.H. (2008). Structural basis for the coevolution of a viral RNA-protein complex. Nat. Struct. Mol. Biol. *15*, 103–105. https://doi.org/10.1038/nsmb1327.

Czaplinski, K. (2017). Techniques for single-molecule mRNA imaging in living cells. In Neuroepigenomics in Aging and Disease, R. Delgado-Morales, ed. (Springer International Publishing), pp. 425–441. https://doi.org/10.1007/978-3-319-53889-1_22.

Ferguson, M.L., and Larson, D.R. (2013). Measuring transcription dynamics in living cells using fluctuation analysis. In Imaging Gene Expression: Methods and Protocols, Y. Shav-Tal, ed. (Humana Press), pp. 47–60. https://doi.org/10.1007/978-1-62703-526-2_4.

Forero-Quintero, L.S., Raymond, W., Handa, T., Saxton, M.N., Morisaki, T., Kimura, H., Bertrand, E., Munsky, B., and Stasevich, T.J. (2021). Live-cell imaging reveals the spatiotemporal organization of endogenous RNA polymerase II phosphorylation at a single gene. Nat. Commun. *12*, 3158. https://doi.org/10.1038/s41467-021-23417-0.

Fusco, D., Accornero, N., Lavoie, B., Shenoy, S.M., Blanchard, J.-M., Singer, R.H., and Bertrand, E. (2003). Single mRNA molecules demonstrate probabilistic movement in living mammalian cells. Curr. Biol. *13*, 161–167. https://doi.org/10.1016/s0960-9822(02)01436-7.

Golding, I., and Cox, E.C. (2004). RNA dynamics in live Escherichia coli cells. Proc. Natl. Acad. Sci. U S A *101*, 11310–11315. https://doi.org/10.1073/pnas.0404443101.

Grünwald, D., and Singer, R.H. (2010). In vivo imaging of labelled endogenous β-actin mRNA during nucleocytoplasmic transport. Nature *467*, 604–607. https://doi.org/10.1038/nature09438.

Halstead, J.M., Lionnet, T., Wilbertz, J.H., Wippich, F., Ephrussi, A., Singer, R.H., and Chao, J.A. (2015). An RNA biosensor for imaging the first round of translation from single cells to living animals. Science *347*, 1367–1671. https://doi.org/10.1126/science.aaa3380.

Heinrich, S., Sidler, C.L., Azzalin, C.M., and Weis, K. (2017). Stem-loop RNA labeling can affect nuclear and cytoplasmic mRNA processing. RNA *23*, 134–141. https://doi.org/10.1261/rna.057786.116.

Horvathova, I., Voigt, F., Kotrys, A.V., Zhan, Y., Artus-Revel, C.G., Eglinger, J., Stadler, M.B., Giorgetti, L., and Chao, J.A. (2017). The dynamics of mRNA turnover revealed by single-molecule imaging in single cells. Mol. Cell *68*, 615–625.e9. https://doi.org/10.1016/j.molcel.2017.09.030.

Huh, D., and Paulsson, J. (2011a). Non-genetic heterogeneity from stochastic partitioning at cell division. Nat. Genet. *43*, 95–100. https://doi.org/10.1038/ng.729.

Huh, D., and Paulsson, J. (2011b). Random partitioning of molecules at cell division. Proc. Natl. Acad. Sci. U S A *108*, 15004–15009. https://doi.org/10.1073/pnas.1013171108.

Jaqaman, K., Loerke, D., Mettlen, M., Kuwata, H., Grinstein, S., Schmid, S.L., and Danuser, G. (2008). Robust single-particle tracking in live-cell time-lapse sequences. Nat. Methods *5*, 695–702. https://doi.org/10.1038/nmeth.1237.

Kahana, C., Asher, G., and Shaul, Y. (2005). Mechanisms of protein degradation: an odyssey with ODC. Cell Cycle *4*, 1461–1464. https://doi.org/10.4161/cc.4.11.2115.

Katz, N., Tripto, E., Granik, N., Goldberg, S., Atar, O., Yakhini, Z., Orenstein, Y., and Amit, R. (2021). Overcoming the design, build, test bottleneck for synthesis of nonrepetitive protein-RNA cassettes. Nat. Commun. *12*, 1576. https://doi.org/10.1038/s41467-021-21578-6.

Katz, Z.B., English, B.P., Lionnet, T., Yoon, Y.J., Monnier, N., Ovryn, B., Bathe, M., and Singer, R.H. (2016). Mapping translation 'hot-spots' in live cells by tracking single molecules of mRNA and ribosomes. Elife *5*, e10415. https://doi.org/10.7554/eLife.10415.

Khuperkar, D., Hoek, T.A., Sonneveld, S., Verhagen, B.M.P., Boersma, S., and Tanenbaum, M.E. (2020). Quantification of mRNA translation in live cells using single-molecule imaging. Nat. Protoc. *15*, 1371–1398. https://doi.org/10.1038/s41596-019-0284-x.

Kowalczyk, G.J., Cruz, J.A., Guo, Y., Zhang, Q., Sauerwald, N., and Lee, R.E.C. (2021). dNEMO: a tool for quantification of mRNA and punctate structures in time-lapse images of single cells. Bioinformatics *37*, 677–683. https://doi.org/10.1093/bioinformatics/btaa874.

Larson, D.R., Zenklusen, D., Wu, B., Chao, J.A., and Singer, R.H. (2011). Real-time observation of transcription initiation and elongation on an endogenous yeast gene. Science *332*, 475–478. https://doi.org/10.1126/science.1202142.

Lenstra, T.L., and Larson, D.R. (2016). Single-molecule mRNA detection in live yeast. Curr. Protoc. Mol. Biol. *113*, 14–24. https://doi.org/10.1002/0471142727.mb1424s113.

Levy, S.F., Ziv, N., and Siegal, M.L. (2012). Bet hedging in yeast by heterogeneous, age-correlated expression of a stress protectant. PLoS Biol. *10*, e1001325. https://doi.org/10.1371/journal.pbio.1001325.

Lim, F., and Peabody, D.S. (2002). RNA recognition site of PP7 coat protein. Nucleic Acids Res. *30*, 4138–4144. https://doi.org/10.1093/nar/gkf552.

Lutje Hulsik, D., Liu, Y.-y., Strokappe, N.M., Battella, S., El Khattabi, M., McCoy, L.E., Sabin, C., Hinz, A., Hock, M., Macheboeuf, P., et al. (2013). A gp41 MPER-specific llama VHH requires a hydrophobic CDR3 for neutralization but not for antigen recognition. Plos Pathog. *9*, e1003202. https://doi.org/10.1371/journal.ppat.1003202.

Ma, H., Tu, L.-C., Naseri, A., Chung, Y.-C., Grunwald, D., Zhang, S., and Pederson, T. (2018). CRISPR-Sirius: RNA scaffolds for signal amplification in genome imaging. Nat. Methods *15*, 928–931. https://doi.org/10.1038/s41592-018-0174-0.

Mateju, D., Eichenberger, B., Voigt, F., Eglinger, J., Roth, G., and Chao, J.A. (2020). Single-molecule imaging reveals translation of mRNAs localized to stress granules. Cell *183*, 1801–1812.e13. https://doi.org/10.1016/j.cell.2020.11.010.

Moon, S.L., Morisaki, T., Khong, A., Lyon, K., Parker, R., and Stasevich, T.J. (2019). Multicolour single-molecule tracking of mRNA interactions with RNP granules. Nat. Cell Biol. *21*, 162–168. https://doi.org/10.1038/s41556-018-0263-4.

Mor, A., Suliman, S., Ben-Yishay, R., Yunger, S., Brody, Y., and Shav-Tal, Y. (2010). Dynamics of single mRNP nucleocytoplasmic transport and export through the nuclear pore in living cells. Nat. Cell Biol. *12*, 543–552. https://doi.org/10.1038/ncb2056.

Morfill, J., Blank, K., Zahnd, C., Luginbühl, B., Kühner, F., Gottschalk, K.-E., Plückthun, A., and Gaub, H.E. (2007). Affinity-matured recombinant antibody fragments analyzed by single-molecule force spectroscopy. Biophys. J. *93*, 3583–3590. https://doi.org/10.1529/biophysj.107.112532.

Pichon, X., Lagha, M., Mueller, F., and Bertrand, E. (2018). A growing toolbox to image gene expression in single cells: sensitive approaches for demanding challenges. Mol. Cell *71*, 468–480. https://doi.org/10.1016/j.molcel.2018.07.022.

Qin, J.Y., Zhang, L., Clift, K.L., Hulur, I., Xiang, A.P., Ren, B.-Z., and Lahn, B.T. (2010). Systematic comparison of constitutive promoters and the doxycycline-inducible promoter. PLoS One *5*, e10611. https://doi.org/10.1371/journal.pone.0010611.

Raj, A., and Tyagi, S. (2010). Chapter 17 - detection of individual endogenous RNA transcripts in situ using multiple singly labeled probes. In Methods in Enzymology, N.G. Walter, ed. (Academic Press), pp. 365–386. https://doi.org/10.1016/S0076-6879(10)72004-8.

Rath, A.K., and Rentmeister, A. (2015). Genetically encoded tools for RNA imaging in living cells. Curr. Opin. Biotechnol. *31*, 42–49. https://doi.org/10.1016/j.copbio.2014.07.012.

Saroufim, M.-A., Bensidoun, P., Raymond, P., Rahman, S., Krause, M.R., Oeffinger, M., and Zenklusen, D. (2015). The nuclear basket mediates perinuclear mRNA scanning in budding yeast. J. Cell Biol. *211*, 1131–1140. https://doi.org/10.1083/jcb.201503070.

Sato, H., Das, S., Singer, R.H., and Vera, M. (2020). Imaging of DNA and RNA in living eukaryotic cells to reveal spatiotemporal dynamics of gene expression. Annu. Rev. Biochem. *89*, 159–187. https://doi.org/10.1146/annurev-biochem-011520-104955.

Schwanhäusser, B., Busse, D., Li, N., Dittmar, G., Schuchhardt, J., Wolf, J., Chen, W., and Selbach, M. (2011). Global quantification of mammalian gene expression control. Nature *473*, 337–342. https://doi.org/10.1038/nature10098.

Shlyakhtina, Y., Moran, K.L., and Portal, M.M. (2019). Asymmetric inheritance of cell fate determinants: focus on RNA. Non-Coding RNA *5*, 38. https://doi.org/10.3390/ncrna5020038.

Skamagki, M., Wicher, K.B., Jedrusik, A., Ganguly, S., and Zernicka-Goetz, M. (2013). Asymmetric localization of Cdx2 mRNA during the first cell-fate decision in early mouse development. Cell Rep. *3*, 442–457. https://doi.org/10.1016/j.celrep.2013.01.006.

Spille, J.H., and Kubitscheck, U. (2015). Labelling and imaging of single endogenous messenger RNA particles in vivo. J. Cell Sci. *128*, 3695–3706. https://doi.org/10.1242/jcs.166728.

Stahl, T., Hümmer, S., Ehrenfeuchter, N., Mittal, N., Fucile, G., and Spang, A. (2019). Asymmetric distribution of glucose transporter mRNA provides a growth advantage in yeast. EMBO J. *38*, e100373. https://doi.org/10.15252/embj.2018100373.

Stothard, P. (2000). The sequence manipulation suite: JavaScript programs for analyzing and formatting protein and DNA sequences. BioTechniques *28*, 1102–1104. https://doi.org/10.2144/00286ir01.

Sunchu, B., and Cabernard, C. (2020). Principles and mechanisms of asymmetric cell division. Development *147*, dev167650. https://doi.org/10.1242/dev.167650.

Tanenbaum, M.E., Gilbert, L.A., Qi, L.S., Weissman, J.S., and Vale, R.D. (2014). A protein-tagging system for signal amplification in gene expression and fluorescence imaging. Cell *159*, 635–646. https://doi.org/10.1016/j.cell.2014.09.039.

Tani, H., Mizutani, R., Salam, K.A., Tano, K., Ijiri, K., Wakamatsu, A., Isogai, T., Suzuki, Y., and Akimitsu, N. (2012). Genome-wide determination of RNA stability reveals hundreds of short-lived noncoding transcripts in mammals. Genome Res. *22*, 947–956. https://doi.org/10.1101/gr.130559.111.

Tantale, K., Mueller, F., Kozulic-Pirher, A., Lesne, A., Victor, J.-M., Robert, M.-C., Capozi, S., Chouaib, R., Bäcker, V., Mateos-Langerak, J., et al. (2016). A single-molecule view of transcription reveals convoys of RNA polymerases and multi-scale bursting. Nat. Commun. *7*, 12248. https://doi.org/10.1038/ncomms12248.

Tutucci, E., Livingston, N.M., Singer, R.H., and Wu, B. (2018a). Imaging mRNA in vivo, from birth to death. Annu. Rev. Biophys. *47*, 85–106. https://doi.org/10.1146/annurev-biophys-070317-033037.

Tutucci, E., Vera, M., Biswas, J., Garcia, J., Parker, R., and Singer, R.H. (2018b). An improved MS2 system for accurate reporting of the mRNA life cycle. Nat. Methods *15*, 81–89. https://doi.org/10.1038/nmeth.4502.

Tutucci, E., Vera, M., and Singer, R.H. (2018c). Single-mRNA detection in living S. cerevisiae using a re-engineered MS2 system. Nat. Protoc. *13*, 2268–2296. https://doi.org/10.1038/s41596-018-0037-2.

Varela, N., Aranguiz, A., Lizama, C., Sepulveda, H., Antonelli, M., Thaler, R., Moreno, R.D., Montecino, M., Stein, G.S., van Wijnen, A.J., and Galindo, M. (2016). Mitotic inheritance of mRNA facilitates translational activation of the osteogenic-lineage commitment factor Runx2 in progeny of osteoblastic cells. J. Cell Physiol. *231*, 1001–1014. https://doi.org/10.1002/jcp.25188.

Vargas, D.Y., Shah, K., Batish, M., Levandoski, M., Sinha, S., Marras, S.A., Schedl, P., and Tyagi, S. (2011). Single-molecule imaging of transcriptionally coupled and uncoupled splicing. Cell *147*, 1054–1065. https://doi.org/10.1016/j.cell.2011.10.024.

Vera, M., Biswas, J., Senecal, A., Singer, R.H., and Park, H.Y. (2016). Single-cell and single-molecule analysis of gene expression regulation. Annu. Rev. Genet. *50*, 267–291. https://doi.org/10.1146/annurev-genet-120215-034854.

Vítor, A.C., Sridhara, S.C., Sabino, J.C., Afonso, A.I., Grosso, A.R., Martin, R.M., and de Almeida, S.F. (2019). Single-molecule imaging of transcription at damaged chromatin. Sci. Adv. *5*, eaau1249. https://doi.org/10.1126/sciadv.aau1249.

Voigt, F., Zhang, H., Cui, X.A., Triebold, D., Liu, A.X., Eglinger, J., Lee, E.S., Chao, J.A., and Palazzo, A.F. (2017). Single-molecule quantification of translation-dependent association of mRNAs with the endoplasmic reticulum. Cell Rep. *21*, 3740–3753. https://doi.org/10.1016/j.celrep.2017.12.008.

Wan, Y., Anastasakis, D.G., Rodriguez, J., Palangat, M., Gudla, P., Zaki, G., Tandon, M., Pegoraro, G., Chow, C.C., Hafner, M., and Larson, D.R. (2021). Dynamic imaging of nascent RNA reveals general principles of transcription dynamics and stochastic splice site selection. Cell *184*, 2878–2895.e20. https://doi.org/10.1016/j.cell.2021.04.012.

Wang, C., Han, B., Zhou, R., and Zhuang, X. (2016). Real-time imaging of translation on single mRNA transcripts in live cells. Cell *165*, 990–1001. https://doi.org/10.1016/j.cell.2016.04.040.

Weber-Bornhauser, S., Eggenberger, J., Jelesarov, I., Bernard, A., Berger, C., and Bosshard, H.R. (1998). Thermodynamics and kinetics of the reaction of a single-chain antibody fragment (scFv) with the leucine zipper domain of

transcription factor GCN4. Biochemistry *37*, 13011–13020. https://doi.org/10.1021/bi980874m.

Wilbertz, J.H., Voigt, F., Horvathova, I., Roth, G., Zhan, Y., and Chao, J.A. (2019). Single-molecule imaging of mRNA localization and regulation during the integrated stress response. Mol. Cell *73*, 946–958.e7. https://doi.org/10.1016/j.molcel.2018.12.006.

Wörn, A., Auf der Maur, A., Escher, D., Honegger, A., Barberis, A., and Plückthun, A. (2000). Correlation between in vitro stability and in vivo performance of anti-GCN4 intrabodies as cytoplasmic inhibitors. J. Biol. Chem. *275*, 2795–2803. https://doi.org/10.1074/jbc.275.4.2795.

Wu, B., Chao, J.A., and Singer, R.H. (2012). Fluorescence fluctuation spectroscopy enables quantitative imaging of single mRNAs in living cells. Biophys. J. *102*, 2936–2944. https://doi.org/10.1016/j.bpj.2012.05.017.

Wu, B., Eliscovich, C., Yoon, Y.J., and Singer, R.H. (2016). Translation dynamics of single mRNAs in live cells and neurons. Science *352*, 1430–1435. https://doi.org/10.1126/science.aaf1084.

Yan, X., Hoek, T.A., Vale, R.D., and Tanenbaum, M.E. (2016). Dynamics of translation of single mRNA molecules in vivo. Cell *165*, 976–989. https://doi.org/10.1016/j.cell.2016.04.034.

CellPress
OPEN ACCESS

STAR★METHODS

KEY RESOURCES TABLE

REAGENT or RESOURCE	SOURCE	IDENTIFIER
Antibodies		
monoclonal antibody to GCN4	Absolute Antibody	C11L34
Chemicals, peptides, and recombinant proteins		
Recombinant human TNF-α	Peprotech	Cat#: 300-01A
Lithium chloride solution	Sigma-Aldrich	Cat#: L-7026
Fugene HD	Promega	Cat#: E2311
Critical commercial assays		
Stellaris® Design Ready probes mCherry with Quasar® 670 Dye	Biosearch^{TM} technologies	VSMF-1031-5
Experimental models: Cell lines		
Human: HeLa cell	ATCC	RRID: CVCL_0030
Human: A549 lung carcinoma cells	ATCC	RRID: CVCL_0023
Recombinant DNA		
cmv-sfgfp-gb1-scAB	This paper	Addgene #185794
cmv-mCherry-8×PP7	This paper	Addgene #185795
cmv-mCherry-10×PP7	This paper	Addgene #185796
ubc-nls-pcp-5×SunTag (SRv.1)	This paper	Addgene #185797
ubc-nls-pcp-10×SunTag (SRv.1.1)	This paper	Addgene #185798
ubc-nls-pcp-12×SunTag (SRv.1.2)	This paper	Addgene #185799
cmv-sfgfp-gb1-scAB-ubc-nls-pcp-5×SunTag (SRv.1-2P)	This paper	Addgene #185800
cmv-sfgfp-gb1-scAB-ubc-nls-pcp-10×SunTag (SRv.1.1-2P)	This paper	Addgene #185801
SRv.1.2-2P (cmv-sfgfp-gb1-scAB-ubc-nls-pcp-12×SunTag)	This paper	Addgene #185802
phage-cmv-cfp-24×ms2	(Wu et al., 2012)	Addgene #40651
phage-cmv-cfp-24×pp7	(Wu et al., 2012)	Addgene #40652
UbC-NLS-HA-MCP-YFP	(Grünwald and Singer, 2010)	Addgene #31230
phage-ubc-nls-ha-pcp-gfp	(Halstead et al., 2015)	Addgene #64539
phage UbiC scAB-GFP	(Voigt et al., 2017)	Addgene #104998
Nb-gp41-Halo	(Boersma et al., 2019)	Addgene #128603
12×MoonTag-12×SunTag-kif18b-24×PP7	(Boersma et al., 2019)	Addgene #128606
pcDNA4TO-5×GCN4_v4-kif18b-24×PP7	(Yan et al., 2016)	Addgene #74927
pcDNA4TO-mito-mCherry-10×GCN4_v4	(Tanenbaum et al., 2014)	Addgene #60914
pET259-pUC57-24×MS2V6	(Tutucci et al., 2018a, 2018b, 2018c)	Addgene #104391
pLH-sgRNA-Sirius-8×PP7	(Ma et al., 2018)	Addgene #121940
CMV-10×PP7 oligo-library based	(Katz et al., 2021)	Addgene #158199
pDZ645 pKAN 1x-mCherry-12×PP7 V4	(Saroufim et al., 2015)	Addgene #73173
Software and algorithms		
ImageJ	(Schneider et al., 2012)	https://imagej.nih.gov/ij/
dNEMO	(Kowalczyk et al., 2021)	https://github.com/recleelab
Python	Python Software Foundation	https://www.python.org
SunRISER modeling scripts	This paper	https://doi.org/10.5281/zenodo.6512459

RESOURCE AVAILABILITY

Lead contact

Requests for resources should be directed to and will be fulfilled by the lead contact, Robin Lee (robinlee@pitt.edu).

Materials availability

Plasmids generated in this study have been deposited to Addgene (plasmid IDs: 185794-185802).

Data and code availability

- All data needed to evaluate the conclusions in the paper are present in the paper and supplementary items.
- All original code been deposited on a Github repository in Zenodo (https://github.com/recleelab/SunRISER_SupplementalModel and https://doi.org/10.5281/zenodo.6512459).
- Any additional information required to reanalyze the data reported in this paper is available from the Lead contact upon request.

EXPERIMENTAL MODEL AND SUBJECT DETAILS

HeLa cells were maintained in DMEM supplemented with 10% fetal bovine serum, 1% streptomycin/penicillin and 1% L-glutamine at 37°C with 5% humidified CO_2.

METHOD DETAILS

Plasmid construction

The 24×SunTag-PCP plasmids were constructed with 24×GCN4 repeats flanked by HindIII and BamHI sites and coat protein flanked by BamHI and EcoRI sites in a pcDNA3 vector. Ubc promoter was PCR amplified from phage-ubc-nls-ha-pcp-gfp (Addgene #64539; (Halstead et al., 2015)) and inserted between MluI and HindIII sites to make ubc-n×SunTag-PCP. 5×SunTag,10×SunTag and 12×SunTag variants were generated by PCR amplification of 5×GCN4, 10×GCN4 and 12×GCN4 from pcDNA4TO-5×GCN4_v4-kif18b-24×PP7 (Addgene #74927 (Bahar Halpern et al., 2015)), pcDNA4TO-mito-mCherry-10×GCN4_v4 (Addgene #60914 (Tanenbaum et al., 2014)) and 12×MoonTag-12×SunTag-kif18b-24×PP7 (Addgene #128606 (Boersma et al., 2019)) and replacing 24×SunTag respectively. SV40NLS, a 57 bp NES signal (ATGAACCTGGTGGACCTCCAAAAGAAGCTGGAGGAGCTGGAGCTGGACGAGCAGCAG) or NES from HIV Rev protein and ODC fragment amplified from pEF-24×V4-ODC-24×PP7 (a gift from Dr. Xiaowei Zhuang's lab) were added at the C-terminus of n×SunTag-PCP between EcoRI and XbaI for various modifications. The ubc-nls-PCP-5×SunTag plasmids were created by replacing gfp sequence in phage-ubc-nls-ha-pcp-gfp with 5×GCN4 flanked by BamHI and BsrGI sites. Similarly, ubc-nls-MCP-5×SunTag were obtained by insertion of 5×GCN4 to UbC-NLS-HA-MCP-YFP (Addgene #31230 (Grünwald and Singer, 2010)) after digestion of XbaI and BsrGI restriction enzymes.

cmv-sfGFP-GB1-scAB was assembled by inserting sfGFP-GB1 fragment from pHRdSV40-scFv-GCN4-sfGFP-VP64-GB1-NLS (Addgene #60904 (Tanenbaum et al., 2014)) and scAB fragment from phage UbiC scAB-GFP (Addgene #104998 (Voigt et al., 2017)) into a pcDNA3 vector.

phage-cmv-cfp-24×ms2 (Addgene #40651 (Wu et al., 2012)) and phage-cmv-cfp-24×pp7 (Addgene #40652 (Wu et al., 2012)) act as reporter mRNA labeled with different stem-loops. 24×MS2V6 stem-loops from pET259-pUC57-24×MS2V6 (Addgene #104391 (Tutucci et al., 2018b);) was amplified using BamHI and SacII sites to label cfp the same way as other two stem-loops. Phage-cmv-mCherry-24×PP7 was obtained by replacing cfp between AgeI and BamHI with mCherry.

For MoonRISE variant, cmv-sfGFP-GB1-Nb-gp41 was created by replacing scAB with Nb-gp41 from Nb-gp41-Halo (MoonTag-Nb-Halo) (Addgene #128603 (Boersma et al., 2019)). Ubc-nls-PCP-12×MoonTag is made by using 12×MoonTag-12×SunTag-kif18b-24×PP7 (Addgene #128606 (Boersma et al., 2019)) as backbone and removing sequences after 12×MoonTag and inserting stop codon and inserting ubc-nls-PCP fragment between SpeI and HindIII sites in front of 12×MoonTag.

cmv-mCherry-12×PP7 was constructed by inserting cmv promoter between NotI and BamHI sites into pDZ645 pKAN 1×-mCherry-12×PP7 V4 (Addgene #73173 (Saroufim et al., 2015)). 8×PP7 and 10×PP7 fragment were amplified from pLH-sgRNA-Sirius-8×PP7 (Addgene #121940 (Ma et al., 2018)) and CMV-10×PP7 oligo-library based (Addgene #158199 (Katz et al., 2021)) respectively and replacing 12×PP7 to create cmv-mCherry-8×PP7 and cmv-mCherry-10×PP7.

Single plasmid encoding SunRISER SR.v1 protein components for SR.v1-2P was produced by ligating PCR amplified cmv-sfGFP-GB1-scFv-bGH poly(A) into ubc-nls-PCP-5×SunTag backbone.

Live cell imaging and quantification of single mRNA spots with dNEMO

HeLa cells were plated on 96-well glass bottom plates (Matriplate) at the density of $8 \times 10^3 \sim 1 \times 10^4$ per well. Transient transfection was performed with Fugene HD (Promega) 24 hrs later according to manufacturer's protocol. A mixture of plasmids comprising SunTag system with equal amount (50 ng) for each was first made in Opti-MEM then Fugene HD was added and incubated for 15 mins at room temperature. The amount of DNA and Fugene HD can be optimized accordingly. 24 hrs after transfection cells

were imaged using a DeltaVision Elite microscope with a 60× objective (1.42 NA; Olympus) and temperature-matched oil in an environmentally controlled chamber (37°C, 5% CO_2). Z-stacks of 5 images with 1 μm interval were acquired for quantification with dNEMO. Cell segmentation was manually performed in dNEMO and the spot detection parameters are set as default. In comparison of SunRISER and MS2-MCP, stacks of 4 planes with a z-spacing of 0.5 μm were obtained for high frame rate (one 3D stack per 2s). For comparison of promoters, mean fluorescence intensity was measured using ImageJ for a fixed region in cytoplasmic area.

Stress treatments

Cells were plated on 96-well glass bottom plates (Matriplate) for fixed-cell and live cell imaging experiments. For perturbation of mitosis, cells were cultured in DMEM with 15 ng/mL TNF, 10 mM LiCl or 5% FBS.

smFISH probes and image acquisition

Five 3′ Cy5 fluorescently labeled DNA oligos (Heinrich et al., 2017) (ggcaattaggtaccttagg, catatcgtctgctcctttc, gagtcgacctgcagggag, atatgctctgctggtttc, atactgcagccagcgagc) as smFISH probes against PP7 stem-loops were synthesized by Genewiz. Stellaris® Design Ready probes mCherry with Quasar® 670 Dye (VSMF-1031-5) against mCherry CDS were synthesized by Biosearch™ technologies. HeLa cells were plated on 96-well glass bottom plates and transfected with SunRISE components for 24 hrs. Cells were then fixed with 3.7% formaldehyde, washed three times in 1xPBS for 5 mins each and permeabilized in 70% (v/v) EtOH overnight at 4°C. The hybridization was then performed overnight at 37°C with 100 nM probes in 2XSSC with 10% formamide and 10% dextran sulfate. Nuclei were labeled in the wash step after the hybridization. Cells were finally imaged in Glox buffer (Raj and Tyagi, 2010) using a 60× objective on a DeltaVision microscope. Z-stack images of both FITC channel (SunRISER) and Cy5 channel (smFISH) were collected.

Fixed-cell immunofluorescence

HeLa cells were plated on 96-well glass bottom plates and transfected with 10×SunTag-PCP or the combination of scAB-GFP and 10×SunTag-PCP for 24hrs. Cells were then fixed with 3.7% formaldehyde for 10 minutes, rinsed three times in 1×PBS for 5 mins each and incubated in 100% methanol for 10 min. Cells were washed three times in PBST (1XPBS 0.1% Tween 20) for 5 mins each and then a primary antibody α-GCN4 (Absolute Antibody C11L34) diluted 1:100 in 3% BSA PBST was applied and incubated overnight at 4°C. After several washes, cells were incubated with secondary antibody (3% BSA PBST with 1:1000 Alexa594-conjugated anti-mouse IgG antibody) for one hour at room temperature. Nuclei were stained in the wash step after secondary antibody. Cells were finally imaged using a 60× objective on a DeltaVision microscope.

QUANTIFICATION AND STATISTICAL ANALYSIS

Statistical analysis

Levene test was performed to calculate p values using raw data from Figure 6B, demonstrating significant changes in the variance of the indicated distributions. Binomial test was used to determine if partitioning of mRNA into daughter cells follows binomial distribution. Two-tailed t tests were performed for calculation of p values for other figures. All analysis is performed with Scipy stats packages in Python.

In Figures 5A, 5B and S8, the same data set is analyzed with the following cell numbers for each condition: 8×PP7-5×ST: n = 8; 8×PP7-10×ST: n = 12; 8×PP7-12×ST: n = 14; 8×PP7-24×ST: n = 9; 10×PP7-5×ST: n = 11; 10×PP7-10×ST: n = 11; 10×PP7-12×ST: n = 10; 10×PP7-24×ST: n = 11; 12×PP7-5×ST: n = 11; 12×PP7-10×ST: n = 14; 12×PP7-12×ST: n = 15; 12×PP7-24×ST: n = 17. In Figures 6C, 6D, S9 and S10, the same dataset is analyzed with the following numbers for mother-daughter pairs: growth medium, LiCl, TNF, low serum are 31, 30, 40 and 32, respectively.

Other number of samples are all listed in figure legends or marked in figures.

Half-life and diffusion constant measurement

HeLa cells transfected with SunRISER for 24hrs was treated with 50μM DRB (5,6-Dichlorobenzimidazole 1-β-D-ribofuranoside, Sigma-Aldrich) and imaged for 10hrs with frame rate of 10 mins. The time course of mRNA counts was fitted to exponential function to extract mRNA half-life $\tau_{1/2} = \ln 2 \times \tau$. For mRNA tracking, fast movie (frame rate of 1.1s) of HeLa cells transfected with SunRISER was taken 24 hrs after transfection and mRNAs were identified with dNEMO and tracked with u-track (Jaqaman et al., 2008). The diffusion constant is calculated as:

$$D = \frac{e^{\gamma/\alpha}}{6}$$

Where γ and α are intercept and slope from linear fit to log-log representation of mean square displacement provided by u-track.

mRNA inheritance during mitosis analysis

HeLa cells were transfected with SunRISER for 24hrs and then cultured in DMEM with TNF (15 ng/mL; Peprotech), LiCl (10 mM; Sigma-Aldrich) or 5% FBS and imaged for 24 hrs after media replacement with a frame rate of 10 mins. mRNA counts are extracted by dNEMO and mother-daughter pairs are manually assigned. The last frame where mother cell remains as a single cell with a semi-detached circular appearance was set as frame 0. The frames −2, −1, 0, of mother cell and 1, 2, 3, of daughter cells are discarded for mRNA quantification because mRNA counts are not accurate during this period due to morphological changes and temporary detachment of the dividing cell. mRNA counts from frames −5, −4, −3, of mother cell and 4, 5, 6 of daughter cells were averaged to represent mRNA abundance before and after division. mRNA relative difference between sister cells is defined as

$$mRNA\ relative\ differences = \frac{|daughter1 - daughter2|}{daughter1 + daughter2}$$

It is noted that daughter1 and daughter2 are randomly assigned so we use absolute value of the difference. mRNA ratio between the sum of post-mitotic sister cells and mother cell is defined as $daughter1 + daughter2$.

Molecular weight calculations

RNA molecular weight was calculated with Quest Calculate™ RNA Molecular Weight Calculator (AAT Bioquest Inc., 2022) and protein molecular weight was calculated with The Sequence Manipulation Suite (Stothard, 2000).

Model-based calculation of signal intensity and signal-to-background values

In the calculation, we assume that all dynamic processes, e.g. the expression of proteins, the transcription of mRNAs and the binding/unbinding of proteins, have reached equilibrium. The dissociation constant of scFv and GCN4, can be written as

$$\kappa_{D1} = \frac{[scFv]\cdot[GCN4]}{[scFv\cdot GCN4]} = \frac{(c_1 - p_1N_1c_2)\cdot(1 - p_1)N_1c_2}{p_1N_1c_2}$$

where c_1 is the molar concentration scFv. c_2 is the molar concentration of PCP-SunTag. N_1 is the number of GCN4 peptides on the PCP-SunTag. p_1 is the probability of a GCN4 binding site occupied by the scFv. Thus, we obtain

$$p_1 = \frac{1}{2N_1c_2}\left(\kappa_{D1} + N_1c_2 + c_1 - \sqrt{(\kappa_{D1} + N_1c_2 + c_1)^2 - 4c_1N_1c_2}\right)$$

Similarly, the probability of a PP7 binding site occupied by a PCP is

$$p_2 = \frac{1}{2N_1c_2}\left(\kappa_{D2} + N_2c_3 + c_2 - \sqrt{(\kappa_{D2} + N_2c_3 + c_2)^2 - 4c_2N_2c_3}\right)$$

Where c_3 is the molar concentration of mRNA, N_2 is the number of PP7 stem-loops on the mRNA, κ_{D2} is the dissociation constant between PCP and PP7.

The number of scFv binding to a single PCP-SunTag satisfies a binomial distribution

$$B_1(n) = \binom{N_1}{n} p_1^n (1 - p_1)^{N_1 - n}$$

Similarly, the number of PCP-SunTag binding to a single mRNA molecule satisfies

$$B_2(m) = \binom{N_1}{m} p_2^n (1 - p_2)^{N_2 - m}$$

The average number of scFv-GFP on a single mRNA molecule is thus

$$\overline{n} = \sum_{m=0}^{N_2}\left(m \cdot B_2(m) \cdot \sum_{n=0}^{N_1} n \cdot B_1(n)\right) = N_1p_1N_2p_2$$

To calculate the distribution of number of scFv-GFP binding to a single mRNA molecule, we first calculate the probability of n scFv-GFP binding to m PCP-SunTag, which is

$$B_1^m(n) = \binom{mN_1}{m} p_1^n (1 - p_2)^{mN_1 - n}$$

Then the probability of n scFv-GFP on a single mRNA molecule is the sum of of all possible m, $B_1^m(n)$ which is

$$P(n) = \sum_{m=0}^{N_2} B_2(m) \cdot B_1^m(n) = \sum_{m=0}^{N_2} \binom{N_2}{m} p_2^m (1-p_2)^{N_2-m} \cdot \binom{mN_1}{n} p_1^n (1-p_1)^{mN_1-n} = (1-p_2)^{N_2} \left(\frac{p_1}{1-p_1}\right) \sum_{n=0}^{N_2} \binom{N_2}{m} \binom{mN_1}{m} \times \left(\frac{p_2}{1-p_2}\right)^m (1-p_1)^{mN_1}$$

Although dissociation constants for variant scFv fragments vary significantly, a value of 0.38 nM (Wörn et al., 2000) was selected for scFV-GCN4 in simulations. We note that modeling results showed similar patterns with optimization at a 5:1 ratio of system components across orders of magnitude in parameter sweeps of the dissociation constant for scFV-GCN4. The dissociation constant for PCP/PP7 is 1 nM (Lim and Peabody, 2002). The dissociation constants for Nb-gp41/MoonTag and MCP/MS2V6 are 30 nM (Lutje Hulsik et al., 2013) and 2.4 nM (Tutucci et al., 2018b).

Considering that the signal from one mRNA molecule will spread to an ellipsoidal area, of which the size is determined by the Rayleigh radius, so we calculate the fluorescence intensity of this area in the presence and without the presence of a single mRNA molecule to calculate signal to noise ratio (SNR). Here, the volume we chose for calculation is V = 200 ×200 ×500 nm. If there is no mRNA in the area, the intensity is defined as the background or noise intensity, I_B. Assuming that the intensity of single GFP-scFv is 1, the background intensity is the sum of free scFv-GFP molecules and the GFP-SunTag-PCP complex

$$I_B = N_A V(c_1 - N_1 p_1 c_2) + N_A V(c_2 - N_2 p_2 c_3) N_1 p_1$$

where N_A is Avogadro constant.

With the intensity of an mRNA molecule as $I_{RNA} = N_1 p_1 N_2 p_2$ the SNR is

$$SNR = \frac{I_{RNA}}{I_B} = \frac{N_1 p_1 N_2 p_2}{N_A V(c_1 - N_1 p_1 c_2) + N_A V(c_2 - N_2 p_2 c_3) N_1 p_1}$$